Overcoming chloride ions-induced deterioration in compressive strength of mortar by graphene oxide

Experimental study and molecular dynamics simulation

Liu, Jialin; Qin, Renyuan; Hu, Ning; Chow, Cheuk Lun; Lau, Denvid

Published in:
Case Studies in Construction Materials

Published: 01/07/2024

Document Version:
Final Published version, also known as Publisher's PDF, Publisher's Final version or Version of Record

Published version (DOI):
10.1016/j.cscm.2024.e03134

Publication details:
Liu, J., Qin, R., Hu, N., Chow, C. L., & Lau, D. (2024). Overcoming chloride ions-induced deterioration in compressive strength of mortar by graphene oxide: Experimental study and molecular dynamics simulation. *Case Studies in Construction Materials*, *20*, Article e03134. https://doi.org/10.1016/j.cscm.2024.e03134

Case Studies in Construction Materials 20 (2024) e03134

Contents lists available at ScienceDirect

Case Studies in Construction Materials

journal homepage: www.elsevier.com/locate/cscm

Overcoming chloride ions-induced deterioration in compressive strength of mortar by graphene oxide: Experimental study and molecular dynamics simulation

Jialin Liu [a,b], Renyuan Qin [c], Ning Hu [d], Cheuk Lun Chow [b], Denvid Lau [b,*]

[a] Key Laboratory of Concrete and Prestressed Concrete Structures of Ministry of Education, Southeast University, Nanjing 210096, China
[b] Department of Architecture and Civil Engineering, City University of Hong Kong, Hong Kong, China
[c] School of Environmental and Civil Engineering, Dongguan University of Technology, Dongguan 523830, China
[d] School of Mechanical Engineering, Hebei University of Technology, Tianjin 300401, China

ARTICLE INFO

Keywords:
Chloride ions
Cementitious materials
Graphene oxide
Experimental study
Molecular dynamics simulations

ABSTRACT

Using seawater to make concrete structures saves freshwater resources and reduces transport costs in offshore construction. However, the presence of chloride ions in mortar causes the formation of Friedel's salt, which changes the microstructure of cement hydration products. As a result, the compressive strength of the mortar significantly deteriorates due to excessive chloride ions. Graphene oxide (GO) is used to overcome chloride ions-induced deterioration in the compressive strength of mortar in this study. The compressive strength of mortar mixed with chloride ions is increased from 38±5.2 MPa to 44.5±0.2 MPa with the addition of GO. Scanning electron microscopy and energy-dispersive X-ray spectroscopy analysis show the decrease of porosity in mortar with GO and adsorption of chloride ions on GO. Molecular dynamics simulations show that GO yields constraints on the mobility of chloride ions and the improvement of interfacial strength between calcium silicate hydrates.

1. Introduction

Fresh water is massively consumed in industrial operations, which is predicted to increase from 800 billion cubic meters in 2009 to a peak of 1,500 billion cubic meters in 2030 [1,2]. The annual consumption of fresh water for concrete production accounts for 18% of the industrial freshwater consumption worldwide [3,4]. To reduce the consumption of fresh water and alleviate the scarcity of freshwater resources, seawater is being used to replace fresh water in concrete production because seawater resources are abundant, given that 71% surface area of the earth is covered by seawater. Besides, using seawater to replace fresh water for concrete production also significantly reduces the transport costs in offshore constructions, such as the buildings in the artificial islands and the ocean platforms [5–7]. The seawater-mixed cementitious materials show improvement in early-age compressive strength compared to the fresh water-mixed cementitious materials because the chloride ions in seawater accelerate the cement hydration rate and result in better early-age compressive strength in fresh concrete [8–10]. However, deterioration occurs in the hardened seawater-mixed cementitious materials (curing for 28 days or longer) [11]. Previous research shows that seawater-mixed concrete shows a 10% deterioration in compressive and tensile strength of hardened concrete curing for 28 days [12]. For steel bar reinforced concrete, the

* Corresponding author.
E-mail address: denvid.lau@cityu.edu.hk (D. Lau).

https://doi.org/10.1016/j.cscm.2024.e03134
Received 10 January 2024; Received in revised form 23 March 2024; Accepted 4 April 2024
Available online 5 April 2024

corrosion of steel bars induced by chloride ions is a detrimental problem [13,14]. However, for concrete without using steel bars, but using fiber reinforced polymer composite, the corrosion of fiber reinforced polymer composite is limited [15,16]. In this situation, the chloride ions in seawater play a pivotal role in the deterioration in compressive strength of the hardened concrete. In the long term, the presence of chloride ions results in the decalcification of cement hydration products by forming calcium chloride through the reaction between sodium chloride solution and calcium hydroxide formed in cement hydration [17], which is highly soluble in water. As a result, the calcium leaching of cement hydration products is accelerated due to the existence of chloride ions [18,19]. Calcium leaching increases porosity and weakens concrete structures. Hence, the compressive strength of concrete deteriorates. In the short term, the chloride ions adsorb on the interlayer of the Aluminate Ferrite mono (AFm) structure, forming Friedel's salt by exchanging the hydroxide ions in AFm [20–22]. Friedel's salt exhibits large sizes and high porosity, filling pores in hardened cementitious materials. Although Friedel's salt fills pores in hardened cementitious materials, the high porosity of Friedel's salt results in low mechanical properties at the location of Friedel's salt, which deteriorates the compressive strength of the hardened cementitious materials [23]. To alleviate the deterioration of chloride ions in the compressive strength of cementitious materials, it is effective to absorb free chloride ions in pore solution in hardened cementitious materials.

Metakaolin is added to ordinary Portland cement to achieve significant improvement in the chloride binding capacity because chloride ions chemically bind to the AFm phase of the cement hydration products [24–26]. Due to the addition of metakaolin, the content of AFm phase is increased [26]. The increased content of AFm reduces the compressive strength of the hardened cementitious materials because the rapid formation of AFm phase at an early age reduces the space for the precipitation of C-S-H [27–29]. Besides, the AFm formation consumes calcium ions during cement hydration and reduces the formation of C-S-H, which also leads to a reduction of the compressive strength of the hardened cementitious materials [30]. To avoid chemical changes in the cement hydration products that reduce the compressive strength of the hardened cementitious materials, GO is used to physically absorb the free chloride ions and overcome the free chloride ions-induced deterioration in the compressive strength of the hardened cementitious materials. The addition of GO with a weight fraction of 0.2% (0.2 wt%) improves the chloride binding capacity of the cement paste by 46% [31]. The desorption of chloride ions from cement hydration product to pore solution due to the reduction of pH value is impeded by adding GO. Specifically, the desorption rate of chloride ions is decreased from 88% to 38% with an addition of 0.2 wt% GO [31]. Besides, the addition of GO significantly refines the pores. It is reported that the addition of 0.04 wt% GO reduces pores in cement paste by 20% [32]. As a result, diffusion of free chloride ions in pore solution in the hardened cementitious materials is restricted. The restricted diffusion of chloride ions impedes the calcium leaching and Friedel's salt formation, which impedes deterioration in the compressive strength of seawater-mixed hardened cementitious materials. However, the role of GO in restricting chloride ions and improving compressive strength of the hardened cementitious materials are unclear.

Experimental approaches and molecular dynamics simulations are widely used to characterize the compressive strength and microstructures of cementitious materials [33,34]. The scanning electron microscope (SEM) images provide a straightforward observation of the morphology of cement hydration products [35,36], which gives insights into the effect of nanomaterials on the pore structure in cementitious materials and the bridging effect of nanomaterials on reinforcing mechanical properties of cementitious materials. Because of the excellent tensile properties of nanomaterials, the failure occurs at the weak interface between the nanomaterials and cementitious materials. The pulled-out failure mode of nanomaterials in cementitious materials is captured by experimental observation [37,38], which indicates that the interfacial shear properties between GO and the cementitious materials are of significance. Energy-dispersive X-ray spectroscopy (EDS) analysis determines the chemical element of the hardened cementitious materials, which is helpful in detecting the affinity of cement hydration products to nanomaterial and studying the role of the affinity to the interfacial properties [39,40]. With the information on the interface from experimental measurements, the atomistic model of the cementitious materials is constructed to study the interfacial properties and microstructural dynamics and the improvement of nanomaterials in compressive strength by molecular dynamics (MD) simulation [41,42]. The interfacial properties between nanomaterials and matrice and underlying mechanisms are effectively explored by MD simulations. The effect of the types of functional groups in GO and water content on the interfacial binding properties between GO and C-S-H are studied by MD simulation [43]. Functional groups result in mechanical interlocking and chemical bonding between GO and C-S-H [44]. The penetration of water molecules decreases the interfacial strength between GO and C-S-H due to the deterioration of hydrogen bonds at the interface between GO and C-S-H indicated by MD simulations [45].

This study aims to use GO to overcome the mechanical deterioration of mortar due to the addition of sodium chloride (NaCl) solutions and give an insight into the underlying mechanisms. The mortar samples are prepared by mixing NaCl into fresh water, cement particles, and river sand. After curing for 28 days, the mortar samples with and without GO are tested under quasi-static compressive loading. The deterioration of chloride ions in the compressive strength of mortar is studied. The influence of GO on the morphology of chloride ions-mixed mortar is studied by SEM tests. The adsorption of chloride ions on GO is studied by EDS analysis. MD simulations are performed to study the adsorption of chloride ions on GO and the role of GO in restricting the chloride ions-induced deterioration in the compressive strength of mortar. The experiments and MD simulations show the effective improvement of GO in compressive strength of chloride ions-mixed mortar, which is of interest to overcome mechanical deterioration, improve the durability of seawater-mixed cementitious materials, and advance the application of seawater to replace fresh water in cementitious materials.

2. Materials and Methods

2.1. Sample preparation and test setup

The Type I ordinary Portland cement 42.5 R is used to prepare mortar samples by mixing with river sand and NaCl solution [41,46]. The concentration of NaCl includes 0 and 3.5%. The maximum concentration is set to 3.5% because the salt concentration in seawater is ~3.5% [12,47]. By adopting different concentrations of NaCl in the mortar, the influence of NaCl on the compressive strength of the mortar is studied. To overcome the degradation in compressive strength induced by chloride ions, GO is added to mortar samples. Industrial GO gel produced by Chengdu Chemicals Co. Ltd., Chinese Academy of Sciences is used in this study. GO gel is a material made from graphene oxide, which is an oxidized form of graphene decorated with oxygen-containing groups on the edges and the basal plane. Specifically, the graphene oxide synthesized by Hummer's method [48] contains epoxide groups, hydroxyl groups, and carboxyl groups. The carboxyl groups are on the edge, and the hydroxyl groups and epoxide groups are on the basal plane [48,49]. The physical properties of the industrial GO gel are listed in Table 1. By mixing, blending, and vibrating the materials, the fresh mortar is obtained with the weight fraction of sodium chloride of 0 and 3.5%. The weight fraction of the mixed materials in mortar samples is shown in Table 2. The weight fraction of GO to the cement is 0.08 wt% because the previous research shows that the addition of 0.08 wt% GO in the cement paste shows excellent reinforcement in the compressive strength [50,51]. Specifically, the compressive strength of cement paste is increased by 42.3, 43.4, 48.5, and 56.3% due to the addition of GO with the weight fraction of 0.02, 0.04, 0.06, and 0.08 wt%, respectively [51]. The slump of the fresh mortar is ~57 mm from the cone height of 300 mm to the mortar height of 243 mm after lifting the slump cone vertically. The fresh mortar shows the true slump, which maintains the shape of the mortar sample and has slight slips. The true slump is desirable because the true slump indicates that the material proportion has appropriate water content and consistency. After curing for 28 days, compressive tests and SEM and EDS analysis are performed on the mortar samples. The compressive test is performed with a loading velocity of 0.01 mm/s. The sample sizes are 100 mm×100 mm×100 mm. The compressive strain rate is 10^{-4}/s, which is an appropriate compressive strain rate because the dynamic strength factor of cementitious materials under a compressive strain rate of 10^{-4}/s is close to the compressive strain rate of 10^{-5}/s in previous research [52].

2.2. Atomistic model construction and simulation details

GO is used to attract the chloride ions in the capillary pores in mortar so that the chloride ions are prevented from reacting with the tricalcium aluminate and forming expanded products. To study the binding properties of chloride ions to GO in the mortar and the interfacial properties between C-S-H gels with/without GO, atomistic models are constructed. Fig. 1a shows the mortar sample at the macroscale. The atomistic configuration of GO and C-S-H gel is shown in Fig. 1b. C-S-H gel is in the dimension of ~50 nm, which is physically bonded by water molecules. In the interlayers of C-S-H gel, water molecules are chemically bonded to the layered structure of C-S-H. GO presents between C-S-H gels with the free water molecules filling the capillary pores. The concentration of chloride ions in the capillary pores varies with the ratio between the weight of chloride and Portland cement used in the mortar sample [53]. The ratio between the weight of chloride and Portland cement is 8.9 wt%. Hence, the concentration of chloride ions in the capillary pores is obtained from previous research [53], which is close to 16%. Hence, the concentration of chloride ions in the atomistic model of GO enhanced C-S-H, as shown in Fig. 1c, is 16%. C-S-H is mimicked by tobermorite because of the similar layered structures and chemical composition in C-S-H and tobermorite, which is also widely used in previous research [54,55]. The sizes of GO-tobermorite model are 45.1 Å, 44.3 Å, and 57.1 Å in *x*-, *y*-, and *z*-direction, respectively. The size of 45.1 Å × 44.3 Å × 57.1 Å is larger than two-fold cutoff distance in MD simulation, which avoids the influence of atoms going through the periodic boundary in *x*-, *y*-, and *z*-direction. Previous research demonstrates that the shear modulus of tobermorite has littile dependence on the sizes of tobermorite. Specifically, the shear modulus of tobermorite with the size of 135.3 Å × 135.9 Å × 135 Å and 45.1 Å × 44.3 Å × 45 Å are 60.3 ± 1.0 GPa and 60.3 ± 0.8 GPa, respectively [56]. Hence, the size of 45.1 Å × 44.3 Å × 45 Å is adopted to construct tobermorite. By inserting water molecules and NaCl into GO in Packmol [57], the GO-tobermorite model is constructed, as shown in Fig. 1c and Fig. 1d.

The accuracy of MD simulations is significantly dependent on the forcefield. The Interface forcefield shows an accurate description of the nanosheet-tobermorite system in previous research [56]. It is reported that MD simulations using an Interface forcefield to describe tobermorite yield a bulk modulus of 71 GPa [58]. The MD simulation results based on the Interface forcefield are close to the bulk moduli of 67 GPa and 69 GPa from density functional theory and measurement, respectively [59,60]. The consistent valence forcefield (CVFF) is widely used to describe the interactions between atoms in GO [61,62]. The parameters of the nonbonded interactions between atoms from tobermorite and GO are extracted from the Interface forcefield and CVFF and calculated by the Lorentz-Berthelot combination rules [58,61].

Table 1
Properties of industrial GO gel.

Type	Purity (wt%)	Thickness (nm)	Diameter (μm)
GO	>97	<5	2–8

Table 2
Weight fraction of mixed materials in mortar samples.

Samples	Water/cement	Sand/cement	NaCl/water	GO/cement
S-0	0.42	2.5	0	0
S-NaCl	0.42	2.5	3.5 wt%	0
S-NaCl-GO	0.42	2.5	3.5 wt%	0.08 wt%

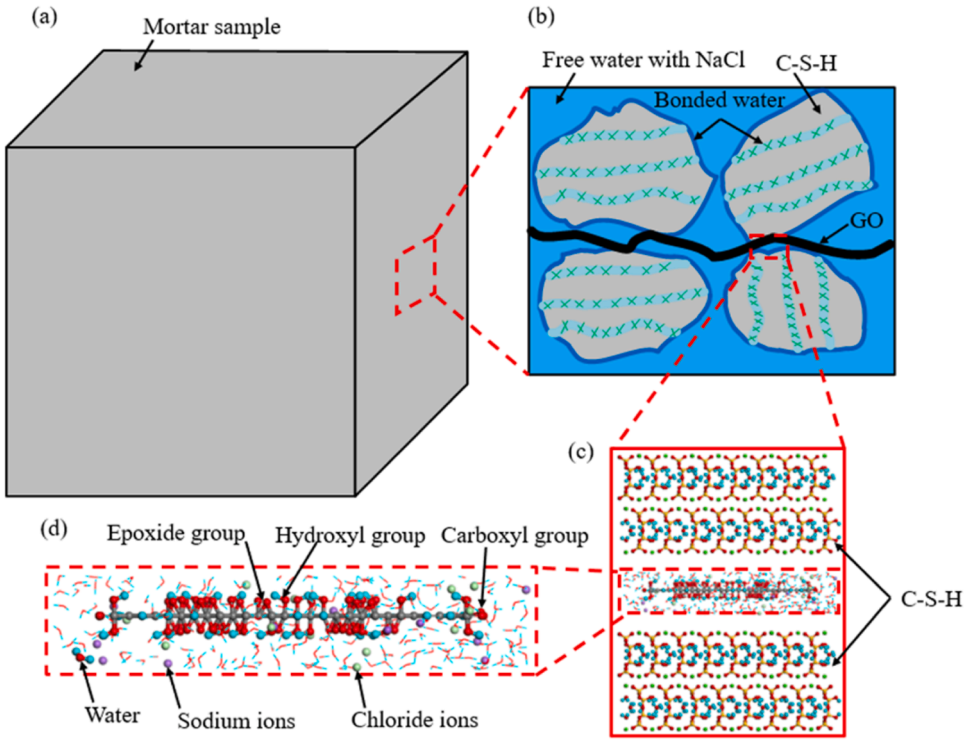

Fig. 1. (a) Macroscale mortar sample, (b) Atomistic configuration of GO and C-S-H gels in mortar sample, (c) atomistic model of GO enhanced C-S-H with the presence of NaCl solution in the capillary pores, (d) Distribution of chloride ions and sodium ions around GO and hydroxyl groups, carboxyl groups, and epoxide groups on GO.

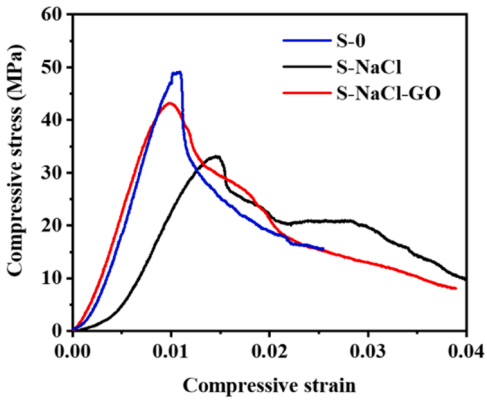

Fig. 2. Compressive stress-strain curves of mortar samples.

3. Results and discussion

3.1. Compressive response of mortar sample

The compressive tests are performed to study the effect of GO on overcoming chloride ions-induced deterioration in the compressive strength of mortar. The typical compressive **s**tress-strain curves of the mortar samples (*i.e.* S-0, S-NaCl, and S-NaCl-GO) are shown in Fig. 2. The experimental results show that the compressive strength of the mortar sample deteriorates significantly due to the addition of chloride ions. Fig. 3 shows that the average strength of the mortar sample S-NaCl with the addition of 3.5% NaCl is 38.0 ±5.2 MPa, which is decreased by 17.7% compared to the pristine mortar sample of 46.2±11.0 MPa without adding NaCl. The deterioration of 17.7% in the compressive strength of mortar is close to previous research. Specifically, the deterioration in compressive strength of mortar is up to 13% due to the addition of seawater in previous research [63]. Whereas the addition of GO improves the compressive strength. The average compressive strength of the mortar sample S-NaCl-GO is 40.6±7.0 MPa, which is increased by 6.8% compared to the average compressive strength of 38.0±5.2 MPa of the mortar sample S-NaCl, as shown in Fig. 3.

Alleviation of chloride ions-induced mechanical deterioration is achieved by the compacted microstructure and the improved chloride binding capacity. Fig. 4a shows the SEM image of the crack bridging in the mortar sample S-NaCl-GO. The EDS spectrum at point 1 in Fig. 4b indicates that GO covered by hydration products is bridging the crack walls when the micro-cracks approaches GO. The bridged micro-cracks are constrained to avoid further opening. Hence, the crack cannot smoothly develop into coarse cracks and the compressive strength of mortar is improved by GO. Besides, the chloride ions are attracted to the surface of GO. As a result, the free chloride ions are restricted to participate in cement hydration and produce Friedel's salt. Hence, the chloride ions-induced deterioration in the compressive strength of the mortar sample is alleviated by GO. Fig. 4c shows the fracture morphology of the mortar sample S-NaCl-GO. At point 2, the EDS spectrum shows that the carbon atom and chloride atom occur, indicating the binding of chloride ions to GO, as shown in Fig. 4d. The binding of chloride ions to GO restricts the formation of cement hydration products that contain chloride ions, such as Friedel's salt. Hence, the mechanical deterioration induced by chloride ions is reduced by adding GO.

3.2. Mobility of chloride ions

To study the effect of GO on the dynamics of chloride ions and the chloride ions binding capacity, the atomistic model is constructed. The mean square displacement (MSD) describes the average value of the square of the atoms' displacement, which helps to understand the movement characteristics of atoms, as well as changes in their positions at different times or under different conditions. Hence, the molecular mobility of chloride ions is quantified by MSD, which is calculated by [61]

$$\mathrm{MSD}_i = \left\langle \left| r_i(t_0 + t) - r_i(t_0) \right|^2 \right\rangle \tag{1}$$

where r_i is the displacement of the atom i, t_0 is the starting time when the displacement of the atom is calculated, t is the time span for calculating the MSD. The angle brackets are used for the average. Compared to the MSD of chloride ions without GO, the MSD of chloride ions is lower with GO, as shown in Fig. 5, which indicates that the presence of GO restricts the mobility of chloride ions in the capillary pores between C-S-H gels.

Due to the presence of GO, the molecular mobility of chloride ions is restricted. The restriction on molecular mobility of chloride ions is beneficial to prevent the adhesion of chloride ions on the cement hydration products and the production of Friedel's salt, which impedes the weakening of the strength development in mortar. The effect of the restriction on the molecular mobility of chloride ions is quantified by the distribution of chloride ions with respect to C-S-H. The oxygen atoms on the surface of C-S-H are close to the capillary pore solution, as shown in Fig. 6a. The radius distribution function (RDF) is a function used to describe the atomic spacing in matter. It represents the probability of finding other particles within a unit-thickness spherical shell at a distance r from the center of a reference particle. Hence, the distribution of chloride ions at a displacement r from oxygen atoms is quantified by RDF. Hence, the radial

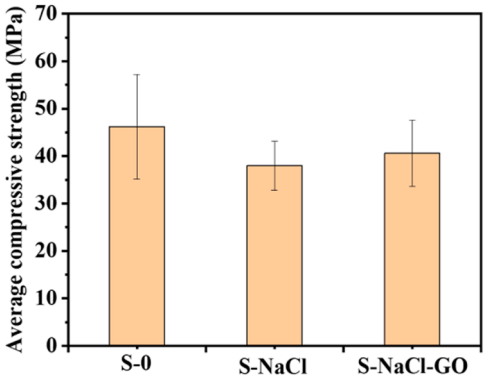

Fig. 3. Average compressive strength of mortar samples.

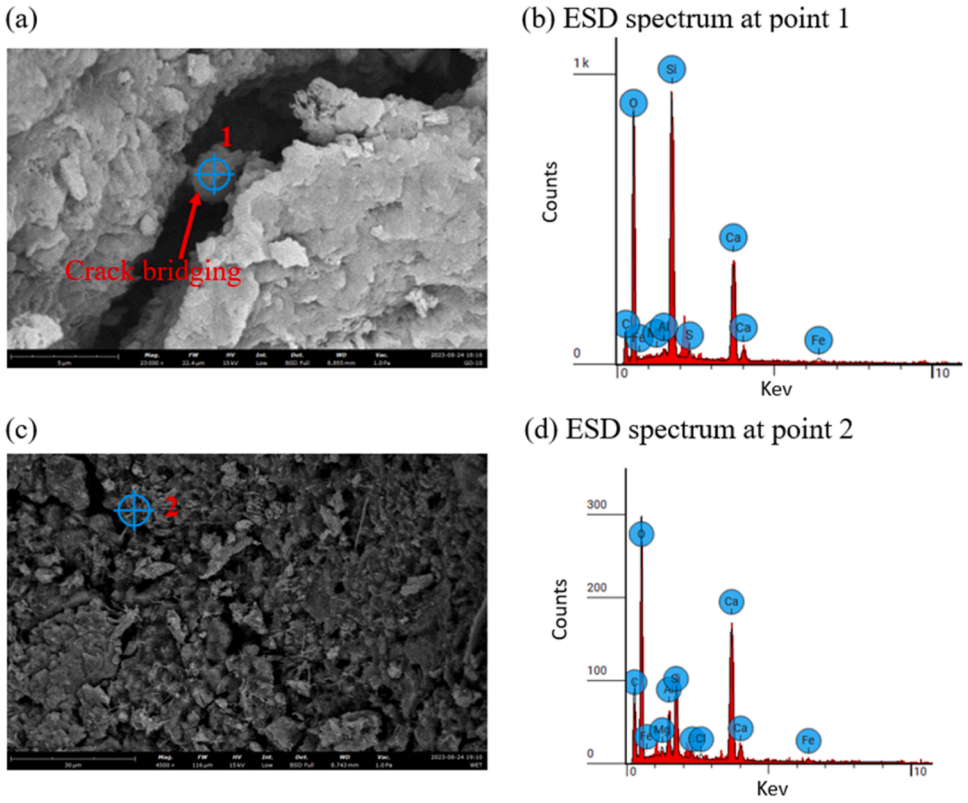

Fig. 4. (a) SEM image of crack bridging in sample S-NaCl-GO, (b) EDS spectrum at spot 1 in sample S-NaCl-GO, and (c) SEM image and (d) EDS spectrum at spot 2 in sample S-NaCl-GO.

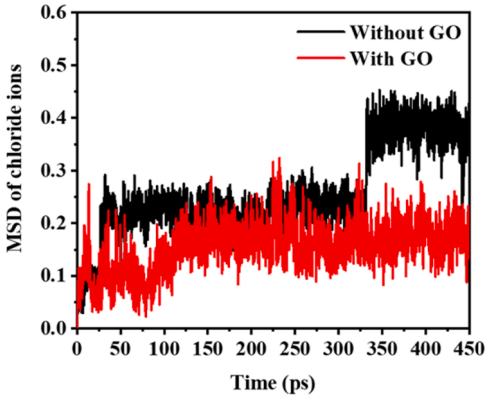

Fig. 5. MSD of chloride ions in capillary pores between C-S-H gels with/without the addition of GO.

distribution function $g_{O-Cl}(r)$ of chloride ions at a displacement r from oxygen atoms in Fig. 6a is calculated by [61]

$$g_{O-Cl}(r) = \frac{\langle N_{O-Cl}(r) \rangle}{\rho \mathrm{d}V(r)} \tag{2}$$

where $N_{O-Cl}(r)$ is the number of chloride ions at a distance between r and $r+\mathrm{d}r$ from oxygen atoms, ρ is the atomic density of the chloride ions at a distance between r and $r+\mathrm{d}r$ from oxygen atoms, $\mathrm{d}V(r)$ is the volume at a distance between r and $r+\mathrm{d}r$ from oxygen atoms, the angle bracket is used to calculate the average. $g_{O-Cl}(r)$ gives insights into the binding capacity of chloride ions with/without GO. The result demonstrates that the radius of the peak value of $g_{O-Cl}(r)$ is different with/without the addition of GO, as shown in Fig. 6b. Without the addition of GO, the radius of the peak value $g_{O-Cl}(r)$ is 3.35 Å. With the addition of GO, the radius of the peak value $g_{O-Cl}(r)$ is 3.65 Å. This discrepancy shows that the distribution of chloride ions is farther to the surface of C-S-H with the addition of GO

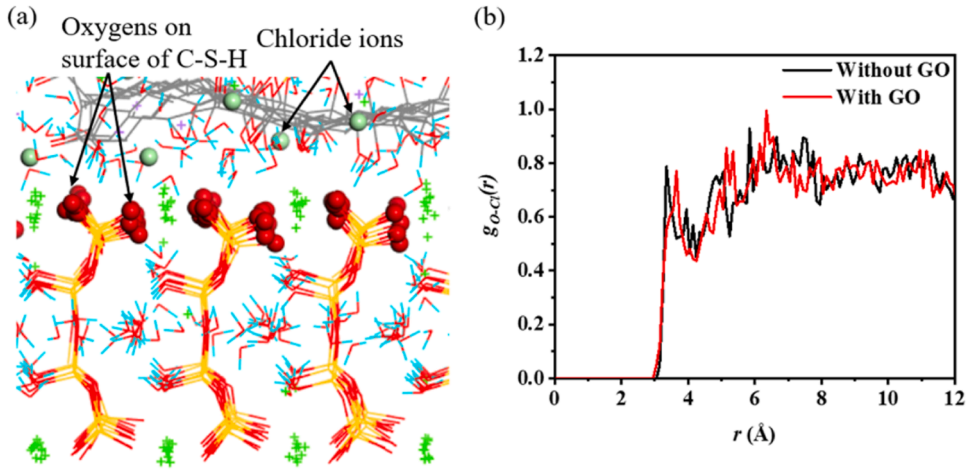

Fig. 6. (a) Geometric configuration of GO and oxygen atoms on the surface of C-S-H. (b) The radial distribution function of chloride ions around the surface of C-S-H with/without the addition of GO.

than without the addition of GO. Hence, the chloride ions are close to the surface of GO, which indicates that the presence of GO attracts chloride ions to GO instead of C-S-H gel. As a result, the presence of GO prevents the adhesion of chloride ions on C-S-H gel and deterioration in the strength development of mortar.

3.3. GO-mortar interfacial properties

The presence of GO provides nucleation sites for C-S-H gels, resulting in the covering of GO by C-S-H gels. Under compressive loading, the C-S-H gels are forced to slide and peel from the neighboring C-S-H gels. To study the improvement of GO in the interfacial properties, the tensile and shear properties between C-S-H gels with and without the addition of GO are studied by MD simulations. The material properties of the tobermorite are sensitive to strain rates in MD simulations. For a large strain rate, the tobermorite is evenly damaged and yields large material properties in tobermorite [64]. When the strain rates decrease, the material properties decrease because the materials have more time to react to the external loading. The weak location (i.e. the interlayer inside the tobermorite) is deteriorated first. When the strain rate decreases to a small magnitude, the material properties of the tobermorite are insensitive to the strain rate. To obtain the small strain rate, different strain rates are applied in the tensile and shear tests in MD simulations from the large to the small, respectively. The simulation results show that the shear and tensile properties at the strain rates of 1×10^{9} s^{-1} and 1×10^{8} s^{-1} are close, respectively. Specifically, the shear moduli of tobermorite are 60.3 ± 0.8 GPa and 58.0 ± 3.2 GPa at shear strain rates of 1×10^{9} s^{-1} and 1×10^{8} s^{-1}, respectively [56]. The tensile strengths of tobermorite are 2.03 GPa and 2.41 GPa at the tensile strain rates of 1×10^{9} s^{-1} and 1×10^{8} s^{-1}, respectively; the tensile moduli of tobermorite are 42.05 GPa and 40.11 GPa at the tensile strain rates of 1×10^{8} s^{-1} and 1×10^{9} s^{-1}, respectively [64]. When the strain rate is decreased from 1×10^{9} s^{-1} to 1×10^{8} s^{-1}, the tensile and shear properties of tobermorite are close, indicating that the material properties of tobermorite are less sensitive to the strain rate at the magnitude of 1×10^{9} s^{-1}. Hence, the strain rates in tension and shear are $10^{9}/s^{-1}$. Fig. 7 shows that the interfacial tensile and shear strengths between C-S-H gels are improved by the addition of GO. The interfacial tensile strength between C-S-H gels is increased by 26.6% from 0.79 GPa to 1.0 GPa with the addition of GO. The interfacial tensile stress-strain curve is changed significantly due to the addition of GO compared to that without the addition of GO, as shown in Fig. 7a. Specifically, without the addition of GO, the interfacial tensile stress drops quickly after the peak stress. With the addition of GO, the interfacial tensile stress drops slowly. This is attributed to the bridging effect of GO between C-S-H gels, as shown in Fig. 8. Under tensile deformation, GO bridging C-S-H gels exhibits excellent interactions with C-S-H gels. The configuration of GO is changed with the variation of tensile strain, as shown in Fig. 8a and Fig. 8b. As a result, GO contributes to the interfacial tensile strength between C-S-H gels. After the peak interfacial tensile stress, GO still bridges C-S-H gels, yielding a slow decrease in the tensile stress, as shown in Fig. 7a. The interfacial shear strength between C-S-H gels is increased by 14.5% from 0.55 GPa to 0.63 GPa with the addition of GO, as shown in Fig. 7b. The shear stress-strain curves in Fig. 7b are close because the water molecules lubricate the interface between the C-S-H gels. Hence, the shear-induced sliding between the C-S-H gels occurs with/without the presence of GO, as shown in Fig. 8a and Fig. 8c. Similar sliding modes yield similar shear stress-strain curves for the C-S-H with/without the presence of GO. The improvement in the interfacial properties between C-S-H gels due to the addition of GO is attributed to the formation of the robust hydrogen bonds between C-S-H gels and functional groups on the surface of GO [43,44,61]. The improved interfacial properties between C-S-H gels account for the improved compressive strength of the mortar sample S-NaCl-GO with GO compared to the mortar sample S-NaCl without GO.

4. Conclusions

This study shows the effect of GO on overcoming chloride ions-induced deterioration in the compressive strength of mortar. The

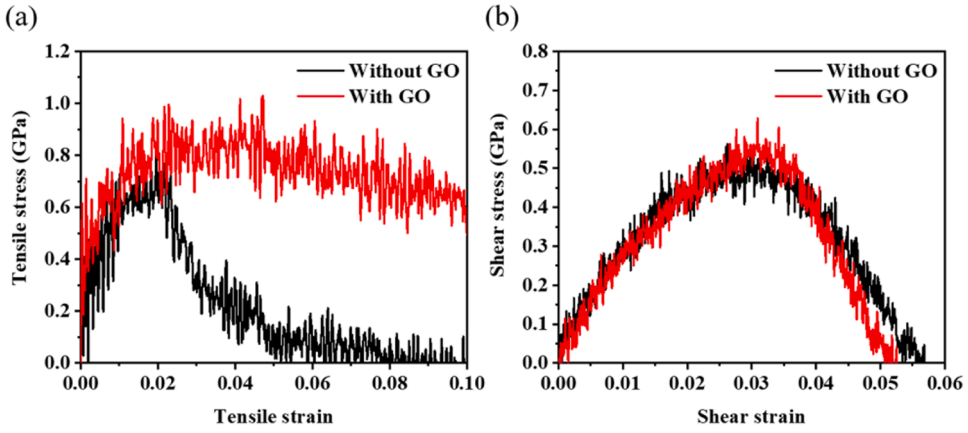

Fig. 7. Interfacial properties between GO and C-S-H under (a) tensile deformation and (b) shear deformation.

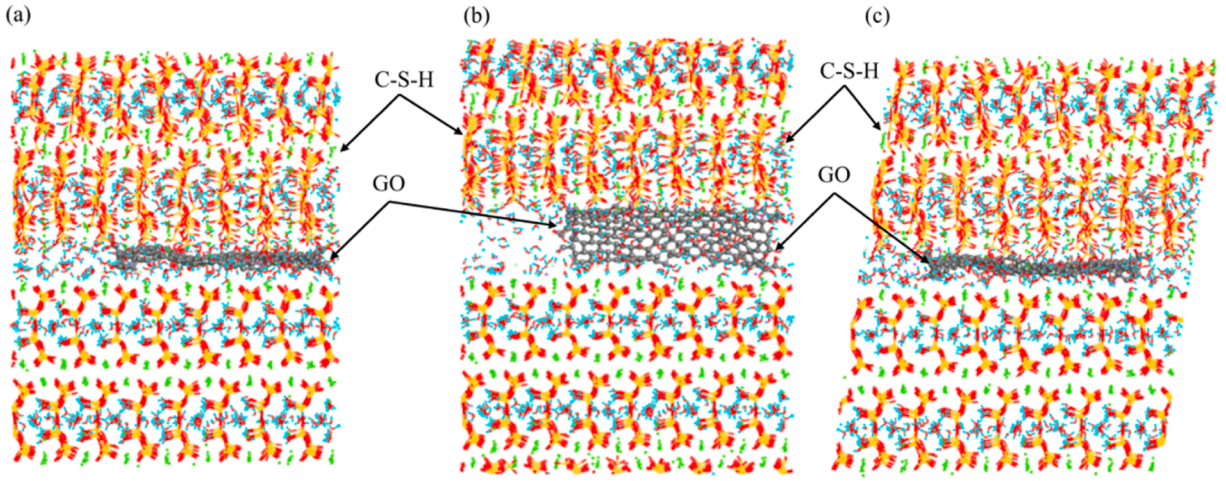

Fig. 8. Configuration of GO between C-S-H: (a) initial atomistic model, (b) deformed model at the tensile strain of 0.1, and (c) the deformed model at the shear strain of 0.05.

compressive strength of mortar samples is decreased from 46.2±11.0 MPa to 38±5.2 MPa due to the addition of 3.5 wt% NaCl during cement hydration. The presence of 0.08 wt% GO significantly increases the compressive strength of mortar mixed with NaCl solution from 38.0±5.2 MPa to 40.6±7.0 MPa. With the addition of GO, the morphology of the mortar sample is physically changed, showing compacted microstructures by SEM analysis. The EDS analysis shows the distribution of chloride ions around GO. Dynamic properties of chloride ions further show that GO effectively restricts the mobility of chloride ions between C-S-H gels by MD simulations, which indicates that the presence of GO restricts the formation of Friedel's salt. Besides, the interfacial tensile and shear strength between C-S-H gels, where chloride ions exist, is also significantly enhanced by adding GO. These findings demonstrate that GO effectively overcomes chloride ions-induced deterioration in compressive strength of mortar, which is attributed to the restriction of GO on the mobility of chloride ions and formation of Friedel's salt, and the enhancement and bridging effect of GO in interfacial properties between C-S-H gels in mortar.

CRediT authorship contribution statement

Denvid Lau: Conceptualization, Funding acquisition, Investigation, Methodology, Project administration, Resources, Supervision, Writing – review & editing. **Ning Hu:** Conceptualization, Writing – review & editing. **Cheuk Lun Chow:** Resources, Supervision, Writing – review & editing. **Jialin Liu:** Writing – original draft, Visualization, Software, Methodology, Investigation, Formal analysis, Data curation, Conceptualization. **Renyuan Qin:** Conceptualization, Data curation, Formal analysis, Investigation, Methodology.

Declaration of Competing Interest

The authors declare that they have no known competing financial interests or personal relationships that could have appeared to

influence the work reported in this paper.

Data Availability

Data will be made available on request.

Acknowledgments

The work described in this paper was fully supported by the grant from the Research Grants Council (RGC) of the Hong Kong Special Administrative Region, China (Project No. CityU 11213022).

References

[1] P.R. de Matos, L.R. Prudêncio Jr, R. Pilar, P.J.P. Gleize, F. Pelisser, Use of recycled water from mixer truck wash in concrete: effect on the hydration, fresh and hardened properties, Constr. Build. Mater. 230 (2020) 116981.
[2] H. Varshney, R.A. Khan, I.K. Khan, Sustainable use of different wastewater in concrete construction: a review, J. Build. Eng. 41 (2021) 102411.
[3] U. Ebead, D. Lau, F. Lollini, A. Nanni, P. Suraneni, T. Yu, A review of recent advances in the science and technology of seawater-mixed concrete, Cem. Concr. Res. 152 (2022) 106666.
[4] S. Saxena, M.H. Baghban, Seawater concrete: a critical review and future prospects, Dev. Built Environ. 16 (2023) 100257.
[5] A. Zhou, R. Qin, C.L. Chow, D. Lau, Structural performance of FRP confined seawater concrete columns under chloride environment, Compos. Struct. 216 (2019) 12–19.
[6] A. Zhou, C.L. Chow, D. Lau, Structural behavior of GFRP reinforced concrete columns under the influence of chloride at casting and service stages, Compos. Part B-Eng. 136 (2018) 1–9.
[7] R. Qin, A. Zhou, D. Lau, Effect of reinforcement ratio on the flexural performance of hybrid FRP reinforced concrete beams, Compos. Part B-Eng. 108 (2017) 200–209.
[8] P. Li, W. Li, T. Yu, F. Qu, V.W.Y. Tam, Investigation on early-age hydration, mechanical properties and microstructure of seawater sea sand cement mortar, Constr. Build. Mater. 249 (2020) 118776.
[9] S.A. Yaseen, G.A. Yiseen, C.S. Poon, Z. Li, Influence of seawater on the morphological evolution and the microchemistry of hydration products of tricalcium silicates (C3S), ACS Sustain. Chem. Eng. 8 (42) (2020) 15875–15887.
[10] J. Wang, E. Liu, L. Li, Multiscale investigations on hydration mechanisms in seawater OPC paste, Constr. Build. Mater. 191 (2018) 891–903.
[11] Y. Sun, J.-X. Lu, C.S. Poon, Strength degradation of seawater-mixed alite pastes: An explanation from statistical nanoindentation perspective, Cem. Concr. Res. 152 (2022) 106669.
[12] A. Younis, U. Ebead, P. Suraneni, A. Nanni, Fresh and hardened properties of seawater-mixed concrete, Constr. Build. Mater. 190 (2018) 276–286.
[13] M. Bazli, J. Dorothea Luck, A. Rajabipour, M. Arashpour, Bond-slip performance of seawater sea sand concrete filled filament wound FRP tubes under cyclic and static loads, Structures 52 (2023) 889–903.
[14] J. Xiao, C. Qiang, A. Nanni, K. Zhang, Use of sea-sand and seawater in concrete construction: Current status and future opportunities, Constr. Build. Mater. 155 (2017) 1101–1111.
[15] K. Zhang, Q. Zhang, J. Xiao, Durability of FRP bars and FRP bar reinforced seawater sea sand concrete structures in marine environments, Constr. Build. Mater. 350 (2022) 128898.
[16] F. Guo, S. Al-Saadi, R.K. Singh Raman, X.L. Zhao, Durability of fiber reinforced polymer (FRP) in simulated seawater sea sand concrete (SWSSC) environment, Corros. Sci. 141 (2018) 1–13.
[17] H. Li, N. Farzadnia, C. Shi, The role of seawater in interaction of slag and silica fume with cement in low water-to-binder ratio pastes at the early age of hydration, Constr. Build. Mater. 185 (2018) 508–518.
[18] M. Zhang, D. Zou, T. Liu, S. Qin, A. Zhou, Calcium leaching mechanism of cementitious materials in the marine environment, J. Mater. Civ. Eng. 35 (6) (2023) 04023122.
[19] A. Delagrave, M. Pigeon, J. Marchand, É. Revertégat, Influence of chloride ions and pH level on the durability of high performance cement pastes (Part II), Cem. Concr. Res. 26 (5) (1996) 749–760.
[20] A.K. Suryavanshi, J.D. Scantlebury, S.B. Lyon, Mechanism of Friedel's salt formation in cements rich in tri-calcium aluminate, Cem. Concr. Res. 26 (5) (1996) 717–727.
[21] Y. Wang, Z. Shui, X. Gao, Y. Huang, R. Yu, Q. Song, Chloride binding capacity and phase modification of alumina compound blended cement paste under chloride attack, Cem. Concr. Compos. 108 (2020) 103537.
[22] D.M. Tadesse, J. Jeon, S. Kim, S. Park, The effect of seawater on the phase assemblage of hydrated cement paste: A study on PC, CAC and CSA, Dev. Built Environ. 15 (2023) 100183.
[23] Y. Zhang, Y. Sun, H. Zheng, Y. Cai, W.L. Lam, C.S. Poon, Mechanism of strength evolution of seawater OPC pastes, Adv. Struct. Eng. 24 (6) (2021) 1256–1266.
[24] M. Gbozee, K. Zheng, F. He, X. Zeng, The influence of aluminum from metakaolin on chemical binding of chloride ions in hydrated cement pastes, Appl. Clay Sci. 158 (2018) 186–194.
[25] A. Machner, M. Zajac, M. Ben Haha, K.O. Kjellsen, M.R. Geiker, K. De Weerdt, Chloride-binding capacity of hydrotalcite in cement pastes containing dolomite and metakaolin, Cem. Concr. Res. 107 (2018) 163–181.
[26] A. Babaahmadi, A. Machner, W. Kunther, J. Figueira, P. Hemstad, K. De Weerdt, Chloride binding in Portland composite cements containing metakaolin and silica fume, Cem. Concr. Res. 161 (2022) 106924.
[27] J. Kim, D. Honda, H. Choi, Y. Hama, Investigation of the relationship between compressive strength and hydrate formation behavior of low-temperature cured cement upon addition of a nitrite-based accelerator, Mater. 12 (23) (2019).
[28] A. Machner, M. Zajac, M. Ben Haha, K.O. Kjellsen, M.R. Geiker, K. De Weerdt, Portland metakaolin cement containing dolomite or limestone-Similarities and differences in phase assemblage and compressive strength, Constr. Build. Mater. 157 (2017) 214–225.
[29] P. Wang, N. Li, L. Xu, Hydration evolution and compressive strength of calcium sulphoaluminate cement constantly cured over the temperature range of 0 to 80°C, Cem. Concr. Res. 100 (2017) 203–213.
[30] T. Dorn, O. Blask, D. Stephan, Acceleration of cement hydration-A review of the working mechanisms, effects on setting time, and compressive strength development of accelerating admixtures, Constr. Build. Mater. 323 (2022) 126554.
[31] W.-J. Long, X. Zhang, G.-L. Feng, J. Xie, F. Xing, B. Dong, J. Zhang, K.H. Khayat, Investigation on chloride binding capacity and stability of Friedel's salt in graphene oxide reinforced cement paste, Cem. Concr. Compos. 132 (2022) 104603.
[32] C. Ruan, J. Lin, S. Chen, K. Sagoe-Crentsil, W. Duan, Effect of graphene oxide on the pore structure of cement paste: implications for performance enhancement, ACS Appl. Nano Mater. 4 (10) (2021) 10623–10633.
[33] K. Cui, K. Liang, T. Jiang, J. Zhang, D. Lau, J. Chang, Understanding the role of carbon nanotubes in low-carbon concrete: from experiment to molecular dynamics, Cem. Concr. Compos. 142 (2023) 105189.
[34] D. Lau, W. Jian, Z. Yu, D. Hui, Nano-engineering of construction materials using molecular dynamics simulations: Prospects and challenges, Compos. Part B-Eng. 143 (2018) 282–291.

[35] K. Cui, D. Lu, T. Jiang, J. Zhang, Z. Jiang, G. Zhang, J. Chang, D. Lau, Understanding the role of carbon nanotubes in low carbon sulfoaluminate cement-based composite, J. Clean. Prod. 416 (2023) 137843.
[36] Z. Zhu, W. Huo, H. Sun, B. Ma, L. Yang, Correlations between unconfined compressive strength, sorptivity and pore structures for geopolymer based on SEM and MIP measurements, J. Build. Eng. 67 (2023) 106011.
[37] W. Wang, S.J. Chen, F. Basquiroto de Souza, B. Wu, W.H. Duan, Exfoliation and dispersion of boron nitride nanosheets to enhance ordinary Portland cement paste, Nanoscale 10 (3) (2018) 1004–1014.
[38] M.A. Rafiee, T.N. Narayanan, D.P. Hashim, N. Sakhavand, R. Shahsavari, R. Vajtai, P.M. Ajayan, Hexagonal boron nitride and graphite oxide reinforced multifunctional porous cement composites, Adv. Funct. Mater. 23 (45) (2013) 5624–5630.
[39] W. Wilson, J.M. Rivera-Torres, L. Sorelli, A. Durán-Herrera, A. Tagnit-Hamou, The micromechanical signature of high-volume natural pozzolan concrete by combined statistical nanoindentation and SEM-EDS analyses, Cem. Concr. Res. 91 (2017) 1–12.
[40] P.T. Durdziński, C.F. Dunant, M.B. Haha, K.L. Scrivener, A new quantification method based on SEM-EDS to assess fly ash composition and study the reaction of its individual components in hydrating cement paste, Cem. Concr. Res. 73 (2015) 111–122.
[41] R. Qin, A. Zhou, Z. Yu, Q. Wang, D. Lau, Role of carbon nanotube in reinforcing cementitious materials: An experimental and coarse-grained molecular dynamics study, Cem. Concr. Res. 147 (2021) 106517.
[42] J. Liu, N. Hu, C.L. Chow, D. Lau, Unfolding behavior of self-folded boron nitride nanosheets inducing ductility of cementitious composites, Appl. Surf. Sci. 599 (2022) 153818.
[43] P. Wang, G. Qiao, Y. Guo, Y. Zhang, D. Hou, Z. Jin, J. Zhang, M. Wang, X. Hu, Molecular dynamics simulation of the interfacial bonding properties between graphene oxide and calcium silicate hydrate, Constr. Build. Mater. 260 (2020) 119927.
[44] M.F. Kai, L.W. Zhang, K.M. Liew, Graphene and graphene oxide in calcium silicate hydrates: Chemical reactions, mechanical behavior and interfacial sliding, Carbon 146 (2019) 181–193.
[45] E. Hosseini, M. Zakertabrizi, A. Habibnejad Korayem, Z. Zaker, R. Shahsavari, Orbital overlapping through induction bonding overcomes the intrinsic delamination of 3D-printed cementitious binders, ACS Nano 14 (8) (2020) 9466–9477.
[46] BS EN 197-1: Cement–Part 1: Composition, specifications and conformity criteria for common cements, European Committee For Standardisation, 2011. London.
[47] J. Antonov, D. Seidov, T. Boyer, R. Locarnini, A. Mishonov, H. Garcia, O. Baranova, M. Zweng, D. Johnson, World Ocean Atlas 2009 Volume 2: Salinity, NOAA Atlas NESDIS 69, in: S. Levitus (Ed.) 184, US Government Printing Office, Washington, DC, 2010.
[48] W.S. Hummers Jr., R.E. Offeman, Preparation of graphitic oxide, J. Am. Chem. Soc. 80 (6) (1958), 1339-1339.
[49] A.H. Cahyana, A.R. Liandi, R.T. Yunarti, D. Febriantini, B. Ardiansah, Green synthesis of dihydropyrimidine based on cinnamaldehyde compound under solvent-free using graphene oxide as catalyst, AIP Conf. Proc. 2168 (1) (2019) 020069.
[50] W. Li, X. Li, S.J. Chen, Y.M. Liu, W.H. Duan, S.P. Shah, Effects of graphene oxide on early-age hydration and electrical resistivity of Portland cement paste, Constr. Build. Mater. 136 (2017) 506–514.
[51] W. Li, X. Li, J. Chen Shu, G. Long, M. Liu Yan, H. Duan Wen, Effects of nanoalumina and graphene oxide on early-age hydration and mechanical properties of cement paste, J. Mater. Civ. Eng. 29 (9) (2017) 04017087.
[52] M.A.A. Abdelrahim, A. Elthakeb, U. Mohamed, M.T. Noaman, Effect of steel fibers and temperature on the mechanical properties of reactive powder concrete, Civ. Eng. Environ. 17 (1) (2021) 270–276.
[53] K.A. Anders, B.P. Bergsma, C.M. Hansson, Chloride concentration in the pore solution of Portland cement paste and Portland cement concrete, Cem. Concr. Res. 63 (2014) 35–37.
[54] J. Liu, N. Hu, C.L. Chow, D. Lau, Water-driven expansion of boron nitride nanosheets for self-healing tobermorite composite, Compos. Sci. Technol. (2023) 109954.
[55] R.J.-M. Pellenq, A. Kushima, R. Shahsavari, K.J. Van Vliet, M.J. Buehler, S. Yip, F.-J. Ulm, A realistic molecular model of cement hydrates, Proc. Natl. Acad. Sci. U.S.A. 106 (38) (2009) 16102–16107.
[56] J. Liu, W. Jian, D. Lau, Boron nitride nanosheet as a promising reinforcement for cementitious composites, Appl. Surf. Sci. 572 (2022) 151395.
[57] L. Martínez, R. Andrade, E.G. Birgin, J.M. Martínez, Software news and update packmol: A package for building initial configurations for molecular dynamics simulations, J. Comput. Chem. 30 (13) (2009) 2157–2164.
[58] R.K. Mishra, A.K. Mohamed, D. Geissbühler, H. Manzano, T. Jamil, R. Shahsavari, A.G. Kalinichev, S. Galmarini, L. Tao, H. Heinz, R. Pellenq, A.C.T. van Duin, S. C. Parker, R.J. Flatt, P. Bowen, cemff: A force field database for cementitious materials including validations, applications and opportunities, Cem. Concr. Res. 102 (2017) 68–89.
[59] R. Shahsavari, M.J. Buehler, R.J.M. Pellenq, F.-J. Ulm, First-principles study of elastic constants and interlayer interactions of complex hydrated oxides: Case study of tobermorite and jennite, J. Am. Ceram. Soc. 92 (10) (2009) 2323–2330.
[60] J.E. Oh, S.M. Clark, H.-R. Wenk, P.J.M. Monteiro, Experimental determination of bulk modulus of 14Å tobermorite using high pressure synchrotron X-ray diffraction, Cem. Concr. Res. 42 (2) (2012) 397–403.
[61] F. Sanchez, L. Zhang, Molecular dynamics modeling of the interface between surface functionalized graphitic structures and calcium-silicate-hydrate: interaction energies, structure, and dynamics, J. Colloid Interface Sci. 323 (2) (2008) 349–358.
[62] H. Wan, Y. Zhang, Interfacial bonding between graphene oxide and calcium silicate hydrate gel of ultra-high performance concrete, Mater. Struct. 53 (2) (2020) 34.
[63] S.K. Kaushik, S. Islam, Suitability of sea water for mixing structural concrete exposed to a marine environment, Cem. Concr. Compos. 17 (3) (1995) 177–185.
[64] J. Zhou, Y. Liang, Effect of water on the dynamic tensile mechanical properties of calcium silicate hydrate: based on molecular dynamics simulation, Mater. 12 (17) (2019) 2837.